The Ternary Silicide $ZrPd_3Si_3$, a Stacking Variant of the α-$FeSi_2$ and Re_3B Structure Types

Meitian Wang and Arthur Mar*

Department of Chemistry, University of Alberta, Edmonton, Alberta, Canada T6G 2G2

Received May 14, 1999. Revised Manuscript Received August 18, 1999

The ternary zirconium palladium silicide $ZrPd_3Si_3$ has been synthesized by arc-melting of the elemental components. It adopts a new structure type and crystallizes in the orthorhombic space group *Cmcm* with $a = 3.8127(4)$ Å, $b = 15.551(1)$ Å, $c = 7.0390(5)$ Å, and $Z = 4$ (Pearson symbol oC28). The structure can be regarded as being built up of Re_3B-type slabs of composition "Pd_3Si" alternating with α-$FeSi_2$ slabs of composition "$ZrSi_2$." Notable features include the presence of Si_2 pairs, square pyramidal and tetrahedral coordination of Pd centers by Si atoms, an unusual distorted cubic coordination of the Zr atoms by the Si_2 pairs, and an extensive network of Zr−Zr, Zr−Pd, and Pd−Pd metal−metal bonds. $ZrPd_3Si_3$ is weakly metallic with a room-temperature resistivity of 1.7×10^{-3} Ω cm. Extended Hückel band structure calculations confirm the metallic behavior; support the simultaneous existence of strong metal−metal, metal−nonmetal, and nonmetal−nonmetal bonding; and suggest a reduced state for the Pd atoms resulting from electron transfer from the Si atoms.

Introduction

Metal silicides are valued for their hardness, chemical inertness, and refractory properties and are involved in applications such as steel production and integrated circuit technology.[1] Many ternary silicides are known, often containing a rare-earth metal or an early transition metal as one component and a late transition metal as another component.[2,3] In systems involving an element from the group 4 triad (Ti, Zr, Hf) and another from the group 10 triad (Ni, Pd, Pt), there exist an impressive number of ternary nickel silicides with diverse crystal structures[4] but surprisingly few palladium or platinum silicides.[5] Of the latter, only the equiatomic phases TiPdSi, ZrPdSi, HfPdSi, ZrPtSi, and HfPtSi are known,[5] all adopting the Co_2Si-type structure.[6] Difficulties in the crystal growth of silicides typically hinder their structural characterization, especially those adopting structure types unrelated to simple ones, and recent efforts in the use of fluxes by others may alleviate this problem.[7] We report here the fortuitous discovery and subsequent rational preparation of $ZrPd_3Si_3$ at high temperature. The novel structure of this compound implies an interesting bonding situation, which is analyzed with the aid of band structure calculations.

Experimental Section

Synthesis. Reagents used were elemental powders of zirconium (99.7%, Cerac), palladium (99.95%, Cerac), silicon (99.96%, Cerac), and antimony (99.995%, Aldrich). $ZrPd_3Si_3$ was originally identified as a side product from a reaction of a 3:3:4 ratio of elemental zirconium, palladium, and antimony in an evacuated silica tube heated at 1000 °C for 3 days, in an attempt to prepare an analogue of $Zr_3Ni_3Sb_4$.[8] On the walls of the tube were found a few black plate-shaped crystals, which were confirmed to contain Zr, Pd, and Si according to an EDX (energy-dispersive X-ray) analysis on a Hitachi F2700 scanning electron microscope. (Anal. (mol %) Calcd: 14% Zr, 43% Pd, 43% Si. Found: 14(1)% Zr, 45(2)% Pd, 41(2)% Si.) Evidently, the incorporation of silicon resulted from an attack of the silica tube at the high temperature used. One of these crystals was selected for the structure determination.

With a knowledge of the correct composition, the ternary silicide was subsequently prepared in a rational manner. A 0.25-g mixture of zirconium, palladium, and silicon in a 1:3:3

(1) *Kirk-Othmer Encyclopedia of Chemical Technology*, 4th ed.; Howe-Grant, M., Ed.; Wiley: New York, 1997.

(2) Parthé, E.; Chabot, B. In *Handbook on the Physics and Chemistry of Rare Earths*; Gschneidner, K. A., Jr., Eyring, L., Eds.; Elsevier: Amsterdam, 1984; Vol. 6; p 113.

(3) Villars, P. *Pearson's Handbook, Desk Edition*; ASM International: Materials Park, OH, 1997.

(4) (a) TiNiSi: Shoemaker, C. B.; Shoemaker, D. P. *Acta Crystallogr.* **1965**, *18*, 900. (b) ZrNiSi, $ZrNi_2Si_2$, $HfNi_2Si_2$: Voroshilov, Yu. V.; Markiv, V. Ya.; Gladyshevskii, E. I. *Inorg. Mater. (Engl. Transl.)* **1967**, *3*, 1224. (c) HfNiSi: Ganglberger, E.; Nowotny, H.; Benesovsky, F. *Monatsh. Chem.* **1967**, *98*, 95. (d) $TiNiSi_2$, $HfNiSi_2$: Markiv, V. Ya.; Gladyshevskii, E. I.; Skolozdra, R. V.; Kripyakevich, P. I. *Dopov. Akad. Nauk. Ukr. RSR, Ser. A: Fiz.-Tekh. Mat. Nauki* **1967**, *(3)*, 266. (e) Ti_2Ni_3Si: Bardos, D. I.; Gupta, K. P.; Beck, P. A. *Trans. Metall. Soc. AIME* **1961**, *221*, 1087. (f) Zr_2Ni_3Si, Hf_2Ni_3Si: Mittal, R. C.; Si, S. K.; Gupta, K. P. *J. Less-Common Met.* **1978**, *60*, 75. (g) $Hf_3Ni_2Si_3$: Yarmolyuk, Ya. P.; Grin′, Yu. N.; Gladyshevskii, E. I. *Sov. Phys. Crystallogr. (Engl. Transl.)* **1977**, *22*, 416. (h) $Zr_2Ni_3Si_4$, $Hf_2Ni_3Si_4$: Yarmolyuk, Ya. P.; Pecharskii, V. K.; Aksel′rud, L. G. *Sov. Phys. Crystallogr. (Engl. Transl.)* **1988**, *33*, 601. (i) $Ti_4Ni_4Si_7$: Horache, E.; Feist, T. P.; Stuart, J. A.; Fischer, J. E. *J. Mater. Res.* **1990**, *5*, 1887. (j) $Zr_5Ni_7Si_{18}$, $Hf_5Ni_9Si_{16}$: Aksel′rud, L. G.; Lysenko, L. A.; Yarmolyuk, Ya. P.; Gladyshevskii, E. I. *Dopov. Akad. Nauk. Ukr. RSR, Ser. A: Fiz.-Mat. Tekh. Nauki* **1977**, *39*, 657. (k) $Ti_6Ni_{16}Si_7$, $Zr_6Ni_{16}Si_7$: Spiegel, F. X.; Bardos, D.; Beck, P. A. *Trans. Metall. Soc. AIME* **1963**, *227*, 575. (l) $Hf_6Ni_{16}Si_7$: Gladyshevskii, E. I. *Sov. Powder Metall. Met. Ceram. (Engl. Transl.)* **1962**, *1*, 262.

(5) (a) TiPdSi: Johnson, V.; Jeitschko, W. *J. Solid State Chem.* **1972**, *4*, 123. (b) ZrPdSi, ZrPtSi[4c] (c) HfPdSi, HfPtSi: Zhao, J. T.; Parthé, E. *J. Less-Common Met.* **1990**, *163*, L7.

(6) Geller, S. *Acta Crystallogr.* **1955**, *8*, 83.

(7) (a) $MNiSi_3$ (M = Sm, Y): Chen, X. Z.; Larson, P.; Sportouch, S.; Brazis, P.; Mahanti, S. D.; Kannewurf, C. R.; Kanatzidis, M. G. *Chem. Mater.* **1999**, *11*, 75. (b) $Ln_2Al_3Si_2$: Chen, X. Z.; Sieve, B.; Henning, R.; Schultz, A. J.; Brazis, P.; Kannewurf, C. R.; Cowen, J. A.; Crosby, R.; Kanatzidis, M. G. *Angew. Chem., Int. Ed. Engl.* **1999**, *38*, 693.

(8) Wang, M.; McDonald, R.; Mar, A. *Inorg. Chem.* **1999**, *38*, 3435.

10.1021/cm990296b CCC: $18.00
Published on Web 10/15/1999

Table 1. Crystallographic Data for $ZrPd_3Si_3$

$ZrPd_3Si_3$	$D_{2h}^{17} - Cmcm$ (No. 63)
fw 494.69	$T = 22$ °C
$a = 3.8127(4)$ Å[a]	$\lambda = 0.71073$ Å
$b = 15.551(1)$ Å[a]	$\rho_{calcd} = 7.873$ g cm^{-3}
$c = 7.0390(5)$ Å[a]	μ(Mo Kα) = 158.0 cm^{-1}
$V = 417.35(6)$ Å^3[a]	$R(F)$ for $F_o^2 > 2\sigma(F_o^2)$[b] = 0.023
$Z = 4$	$R_w(F_o^2)$[c] = 0.047

[a] Based on 24 centered reflections in the range $20° \le 2\theta$(Mo Kα) $\le 42°$, and obtained from a refinement constrained so that $\alpha = \beta = \gamma = 90°$. [b] $R(F) = \sum||F_o| - |F_c||/\sum|F_o|$. [c] $R_w(F_o^2) = [\sum[w(F_o^2 - F_c^2)^2]/\sum wF_o^4]^{1/2}$; $w^{-1} = [\sigma^2(F_o^2) + (0.0185p)^2]$ where $p = [\max(F_o^2,0) + 2F_c^2]/3$.

ratio was pressed into a pellet, which was then melted twice in a Centorr 5TA tri-arc furnace under argon (gettered by melting a titanium pellet). With a few grains of I_2 added, the product of the arc-melting reaction was annealed in a two-zone furnace at 950/900 °C for 4 days. The X-ray powder pattern, obtained on an Enraf-Nonius FR552 Guinier camera (Cu Kα_1 radiation; Si standard), revealed the presence of $ZrPd_3Si_3$, PdSi,[9] and trace amounts of an unidentified impurity. The cell parameters of $ZrPd_3Si_3$, refined with the use of the program POLSQ,[10] are $a = 3.805(1)$ Å, $b = 15.515(5)$ Å, $c = 7.022(2)$ Å, and $V = 414.5(2)$ Å^3. It appears that $ZrPd_3Si_3$ is a metastable phase, since a similar reaction at 950 °C of the elements placed in a niobium tube but in the absence of I_2 results only in the formation of the equiatomic phase ZrPdSi[5b] as well as Pd_2Si.[11] Attempts to substitute Hf for Zr, and Ni or Pt for Pd were unsuccessful under a variety of conditions.

Structure Determination. Weissenberg photography revealed Laue symmetry *mmm* and confirmed the singularity of a crystal selected for data collection. Intensity data were obtained at room temperature with the $\theta-2\theta$ scan technique in the range $5° \le 2\theta$(Mo Kα) $\le 70°$ on an Enraf-Nonius CAD-4 diffractometer. Crystal data and further details of the data collection are given in Table 1 and the Supporting Information. Calculations were carried out with the use of the SHELXTL (Version 5.1) package.[12] Conventional atomic scattering factors and anomalous dispersion corrections were used.[13] Intensity data were processed, and face-indexed absorption corrections were applied in XPREP. Of the possible space groups consistent with the orthorhombic symmetry and systematic absences observed in the intensity data ($Cmc2_1$, $C2cm$, $Cmcm$), the centrosymmetric space group $Cmcm$ was chosen on the basis of the successful structure solution and refinement. Initial positions of all atoms were found by direct methods, and the structure was refined by least-squares methods. Refinements on occupancy factors confirm that all sites are fully occupied. The atomic parameters were standardized with STRUCTURE TIDY.[14] The final cycle of least-squares refinement on F_o^2 of 26 variables (including anisotropic displacement parameters and an isotropic extinction parameter) and 543 averaged reflections (including those having $F_o^2 < 0$) converged to values of $R_w(F_o^2)$ of 0.047 and $R(F)$ (for $F_o^2 > 2\sigma(F_o^2)$) of 0.023. The final difference electron density map is featureless ($\Delta\rho_{max} = 2.15$; $\Delta\rho_{min} = -2.42$ e Å^{-3}). Final values of the positional and equivalent isotropic displacement parameters are given in Table 2, anisotropic displacement parameters and bond angles are in the Supporting Information, and final structure amplitudes are available from the authors. Selected bond distances are listed in Table 3.

Electrical Resistivity. A single crystal of dimensions 0.5 × 0.1 × 0.1 mm, verified to be $ZrPd_3Si_3$ by EDX analysis, was mounted in a four-probe configuration for an ac resistivity measurement between 20 and 290 K. This measurement gives the resistivity along the crystallographic *a* axis.

Band Structure. A three-dimensional tight-binding extended Hückel band structure calculation was performed using the EHMACC suite of programs.[15,16] The weighted Wolfsberg–Helmholz formula for the off-diagonal Hamiltonian matrix elements was employed.[17] The atomic parameters used are listed in Table 4. Properties were extracted from the band structure using 96 *k*-points in the irreducible portion of the Brillouin zone.

Table 2. Positional and Equivalent Isotropic Thermal Parameters (Å^2) for $ZrPd_3Si_3$

atom	Wyckoff position	*x*	*y*	*z*	U_{eq}[a]
Zr	4c	0	0.01166(3)	1/4	0.0056(1)
Pd(1)	8f	0	0.17553(2)	0.55292(4)	0.0068(1)
Pd(2)	4c	0	0.66047(3)	1/4	0.0066(1)
Si(1)	8f	0	0.42602(7)	0.03248(16)	0.0070(2)
Si(2)	4c	0	0.26196(11)	1/4	0.0073(3)

[a] U_{eq} is defined as one-third of the trace of the orthogonalized U_{ij} tensor.

Table 3. Selected Interatomic Distances (Å) and Mulliken Overlap Populations (MOP) for $ZrPd_3Si_3$

	distance (Å)[a]	MOP
	Metal-Nonmetal	
Zr–Si(1)	2.778(1) (×4)	0.309
Zr–Si(1)	2.914(1) (×4)	0.243
Pd(1)–Si(1)	2.4744(9) (×2)	0.200
Pd(1)–Si(2)	2.515(1)	0.228
Pd(1)–Si(2)	2.5447(8) (×2)	0.213
Pd(2)–Si(1)	2.395(1) (×2)	0.251
Pd(2)–Si(2)	2.470(1) (×2)	0.257
	Metal–Metal	
Pd(1)–Pd(1)	2.768(1)	0.030
Pd(1)–Pd(1)	3.0841(8) (×2)	0.009
Pd(1)–Pd(2)	2.8633(6) (×2)	0.023
Pd(1)–Pd(2)	2.8964(9)	0.022
Zr–Pd(1)	3.217(1) (×2)	0.047
Zr–Pd(1)	3.3149(9) (×2)	0.041
Zr–Pd(2)	2.9917(8) (×2)	0.110
Zr–Zr	3.530(1) (x2)	0.104
	Nonmetal–Nonmetal	
Si(1)–Si(1)	2.340(2)	0.685
Si(1)–Si(1)	3.055(2)	0.186
Si(1)–Si(2)	2.969(2)	0.258

[a] Interatomic distances were calculated based on the cell parameters refined from X-ray powder diffraction data.

Table 4. Extended Hückel Parameters

atom	orbital	H_{ii} (eV)	ξ_{i1}	c_1	ξ_{i2}	c_2
Zr	5s	−8.52	1.82			
	5p	−4.92	1.78			
	4d	−8.63	3.84	0.6213	1.510	0.5798
Pd	5s	−7.51	2.19			
	5p	−3.86	2.15			
	4d	−12.53	5.98	0.55	2.61	0.67
Si	3s	−17.3	1.383			
	3p	−9.2	1.383			

Results and Discussion

Although the structure of $ZrPd_3Si_3$ is three-dimensional in nature, it will be helpful to partition it into

(9) Engström, I. *Acta Chem. Scand.* **1970**, *24*, 1466.
(10) POLSQ: Program for least-squares unit cell refinement. Modified by D. Cahen and D. Keszler, Northwestern University, 1983.
(11) Nylund, A. *Acta Chem. Scand.* **1966**, *20*, 2381.
(12) Sheldrick, G. M. SHELXTL Version 5.1; Bruker Analytical X-ray Systems, Inc.: Madison, WI, 1997.
(13) *International Tables for X-ray Crystallography*; Wilson, A. J. C., Ed.; Kluwer: Dordrecht, The Netherlands, 1992; Vol. C.
(14) Gelato, L. M.; Parthé, E. *J. Appl. Crystallogr.* **1987**, *20*, 139.
(15) Whangbo, M.-H.; Hoffmann, R. *J. Am. Chem. Soc.* **1978**, *100*, 6093.
(16) Hoffmann, R. *Solids and Surfaces: A Chemist's View of Bonding in Extended Structures*; VCH Publishers: New York, 1988.
(17) Ammeter, J. H.; Bürgi, H.-B.; Thibeault, J. C.; Hoffmann, R. *J. Am. Chem. Soc.* **1978**, *100*, 3686.

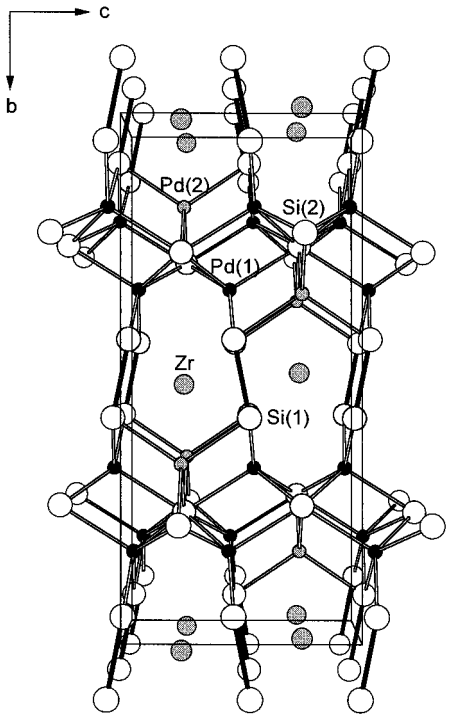

Figure 1. View of $ZrPd_3Si_3$ along the *a* axis showing the unit cell outline and the labeling scheme. The medium lightly shaded circles are Zr atoms, the small solid circles are Pd atoms, and the large open circles are Si atoms. The metal-centered coordination polyhedra are emphasized: Pd(1) square pyramid, Pd(2) tetrahedron, and Zr distorted cube.

component slabs or layers. Figure 1 shows the structure, viewed along the *a* axis, as being built up from three kinds of metal-centered coordination polyhedra whose vertices are the Si atoms. Pd(1) is coordinated in a square pyramidal geometry to two Si(1) atoms at 2.4744(9) Å and two Si(2) atoms at 2.5447(8) Å forming the base, and to a Si(2) atom at 2.515(1) Å forming the apex. Pd(2) is coordinated tetrahedrally to two Si(1) and two Si(2) atoms at 2.395(1) and 2.470(1) Å, respectively, at the expected angles (100.78(7)−111.84(6)°). The Pd square pyramids and tetrahedra share their corners and edges to form a slab aligned parallel to the *ac* plane. These slabs, stacked along the long *b* axis, are joined together through pairing of the Si(1) atoms. The Zr atoms are then positioned in an unusual distorted cubic coordination environment with four short (2.778(1) Å) and four long (2.914(1) Å) distances to the Si(1) atoms.

An alternative description, shown in Figure 2a, emphasizes the relationship of $ZrPd_3Si_3$ to two simpler structure types adopted by binary silicides. Here, $^3_\infty[ZrPd_3Si_3]$ can be partitioned into slabs of composition $^2_\infty[ZrSi_2]$ and $^2_\infty[Pd_3Si]$, which are stacked in an alternating fashion along *b*. Although $ZrSi_2$ itself does not adopt this structure,[18] the slab $^2_\infty[ZrSi_2]$ occurs in the rare α-$FeSi_2$ structure type.[19] It is built up by placing metal atoms in half of the interstices of a cubic array of Si atoms (and may thus be regarded as the cubic analogue of the more familiar hexagonal $Cd(OH)_2$ structure).[20] Similarly, the slab $^2_\infty[Pd_3Si]$ occurs in the Re_3B structure type.[21] In $^2_\infty[Pd_3Si]$, the Si atoms reside

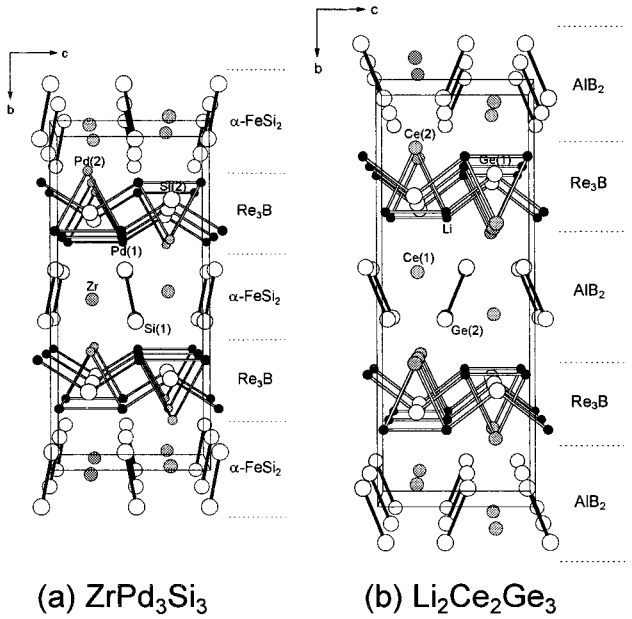

Figure 2. Comparison of the structures of (a) $ZrPd_3Si_3$ and (b) $Li_2Ce_2Ge_3$ viewed along the *a* axis, showing how they are built up of slabs belonging to the Re_3B, α-$FeSi_2$, and AlB_2 structure types. Standardization of the $Li_2Ce_2Ge_3$ structure gives the atomic labeling scheme shown.[14]

at the centers of Pd_6 trigonal prisms that share their triangular faces to form infinite columns. Adjacent columns are shifted half the height of a trigonal prism with respect to each other so that Si atoms achieve a bicapped trigonal prismatic coordination, and the columns are linked together. Pd_3Si[22] itself adopts the Fe_3C structure type,[23] which differs from the Re_3B structure type mainly in the way in which the trigonal prisms are linked.[20] Indeed, trigonal prisms of metal atoms are a common feature in many intermetallic compounds and occur not only in Pd_3Si but also in other binary palladium silicides such as Pd_2Si.[11] Neither $ZrPd_3Si_3$ nor the parent α-$FeSi_2$ and Re_3B structures are themselves layered compounds in the usual sense because strong bonding is present along the stacking direction.

Partitioning the $ZrPd_3Si_3$ structure into component slabs exposes its connection to the closely related $Li_2Ce_2Ge_3$ structure (Figure 2b).[24] A Re_3B-type slab also occurs in the $Li_2Ce_2Ge_3$ structure, but the vertices in the trigonal prisms are made up of two kinds of atoms, Li and Ce(2). Ge_2 pairs in the intervening slabs are tilted in opposite directions in $Li_2Ce_2Ge_3$ relative to those of the Si_2 pairs in $ZrPd_3Si_3$. Equivalently, the α-$FeSi_2$-like slab is translated half a unit cell edge along *c* in $Li_2Ce_2Ge_3$ compared to $ZrPd_3Si_3$. Last, whereas the Zr atoms in $ZrPd_3Si_3$ are located at the centers of cubes formed by eight Si(1) atoms, the corresponding Ce(1) atoms in $Li_2Ce_2Ge_3$ are drastically shifted along *b*. This distortion places the Ge(2) atoms at the centers of trigonal prisms formed by four Ce(1) and two Ce(2) atoms. For this reason, the more natural description for

(18) Schachner, H.; Nowotny, H.; Kudielka, H. *Monatsh. Chem.* **1954**, *85*, 1140.
(19) Aronsson, B. *Acta Chem. Scand.* **1960**, *14*, 1414.
(20) Hyde, B. G.; Andersson, S. *Inorganic Crystal Structures*; Wiley: New York, 1989.
(21) Aronsson, B.; Bäckman, M.; Rundqvist, S. *Acta Chem. Scand.* **1960**, *14*, 1001.
(22) Aronsson, B.; Nylund, A. *Acta Chem. Scand.* **1960**, *14*, 1011.
(23) Herbstein, F. H.; Smuts, J. *Acta Crystallogr.* **1964**, *17*, 1331.
(24) Pavlyuk, V. V.; Pecharskii, V. K.; Bodak, O. I.; Bruskov, V. A. *Sov. Phys. Crystallogr. (Engl. Transl.)* **1988**, *33*, 24.

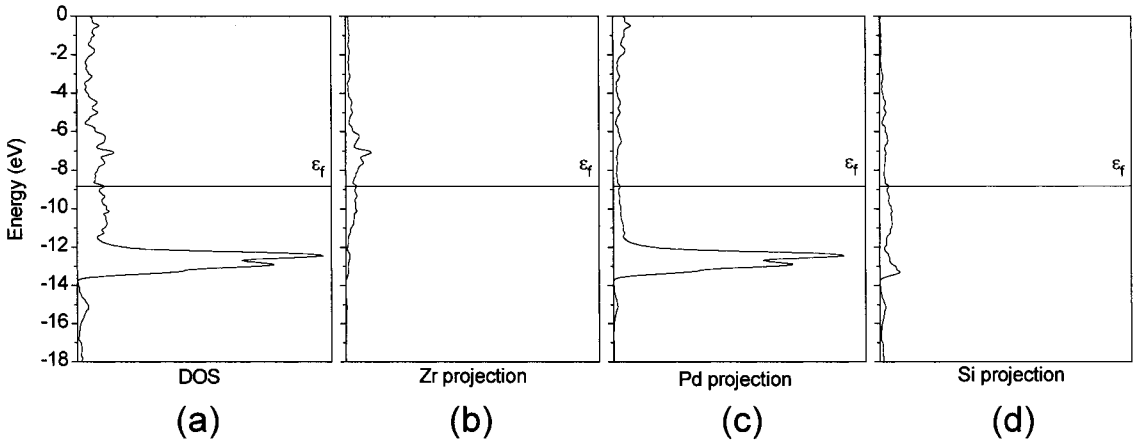

Figure 3. Density of states (DOS) curve for (a) $ZrPd_3Si_3$ and its (b) Zr, (c) Pd, and (d) Si projections. The Fermi level, ϵ_f, is at −8.9 eV.

the $Li_2Ce_2Ge_3$ structure that appears in the literature is as a combination of Re_3B- and AlB_2-type slabs.[24]

Examination of the interatomic distances (Table 3) shows that while the Zr−Si and Pd−Si bonds in $ZrPd_3Si_3$ are normal (cf., 2.682−3.057 Å in $ZrSi_2$[18] and 2.347−2.564 Å in Pd_3Si,[22] respectively), the distinguishing feature is the short distance of 2.340(2) Å within the Si(1)−Si(1) pair. This is essentially identical to the distances found in similar pairs in $MNiSi_3$ (M = Sm, Y) (∼2.34 Å)[7a] and to that in elemental Si (2.3517 Å).[25] At first glance, the electronic distribution in $ZrPd_3Si_3$ seems to be straightforward. Applying Zintl's concept, we assume that Zr, being the most electropositive component, transfers all its valence electrons to become Zr^{+4}. Since Si(1) forms a homonuclear bond with itself and Si(2) does not, the appropriate oxidation numbers are $Si(1)^{-3}$ and $Si(2)^{-4}$. This implies an assignment of +2 for the Pd atoms, resulting in the formulation $(Zr^{+4})(Pd^{+2})_3(Si(1)^{-3})_2(Si(2)^{-4})$. Two observations suggest that the electronic distribution is not as simple as this. First, it is Pd, not Si, that is the most electronegative component in this system (Pauling electronegativities: Zr, 1.4; Pd, 2.2; Si, 1.8).[26] Thus, unlike typical Zintl compounds, electron transfer should occur from the nonmetal, Si, to the metal, Pd. As has been discussed recently, the conventional electron counting scheme fails to give a realistic picture in cases such as these.[27] Second, some of the Zr−Zr, Zr−Pd, and Pd−Pd distances suggest the existence of an extensive metal−metal bonding network within the $ZrPd_3Si_3$ structure. For instance, the Pd(1)−Pd(1) distance forming the base of the isosceles triangles of the Pd_6 trigonal prisms is 2.768(1) Å, only slightly longer than that found in elemental Pd (2.7506 Å).[25]

To interpret the bonding in $ZrPd_3Si_3$ in more detail, a semiempirical band structure calculation was carried out. Reflecting the reversal in electronegativity of the metal and nonmetal, the atomic Si 3p levels start off higher in energy than the Pd 4d levels (see the Hückel parameters used in Table 4). The density of states (DOS) curve (Figure 3) reveals substantial covalent mixing of Zr, Pd, and Si states. Near the Fermi level (ϵ_f = −8.9 eV), all three elements make equally significant contributions to the DOS. Above the Fermi level, the unfilled states have their major contribution from Zr 4d orbitals, so electropositive Zr has transferred some of its electrons to the rest of the structure. The narrow peak from −11.0 to −14.0 eV located well below the Fermi level represents filled states composed almost entirely of Pd 4d character. With all its 4d orbitals fully occupied, it would appear that Pd has a configuration of d^{10} (in accordance with the modified electron counting scheme used in such instances involving weakly electronegative ligands)[27,28] and is either neutral or possibly even negatively charged. Consistent with all these expectations, the calculated charges are +0.144 for Zr, −0.372 for Pd, and +0.324 for Si.

Bonding within $ZrPd_3Si_3$ is highly covalent, and while metal−nonmetal (Zr−Si, Pd−Si) interactions provide the major source of its stability, metal−metal (Zr−Zr, Zr−Pd, Pd−Pd) and nonmetal−nonmetal (Si−Si) interactions play an important role as well. Mulliken overlap populations (MOP) were determined for various contacts in $ZrPd_3Si_3$ to gauge the strength of these interactions and are listed in Table 3. The Zr−Si and Pd−Si interactions account for most of the bonding energy, the average MOP being 0.276 and 0.223, respectively. (For comparison, 2.738−2.868 Å Zr−Si bonds have an average MOP of 0.276 in ZrSi,[18] and 2.4485−2.5710 Å Pd−Si bonds have an average MOP of 0.230 in PdSi.[9])[29] As shown in the crystal orbital overlap population (COOP) curves, the Zr−Si bonding levels are nearly completely filled up to the Fermi level (Figure 4a), while there remain some Pd−Si bonding levels above the Fermi level (Figure 4b). Although Pd−Si bonding has not been maximized in this structure, this is more than compensated by the formation of metal−metal and nonmetal−nonmetal bonds.

The Pd−Pd, Zr−Pd, Zr−Zr, and Si−Si interactions in $ZrPd_3Si_3$ are not negligible. For the Pd(1)−Pd(1) contact alluded to earlier, the filling of metal−metal bonding levels (−13 eV) is nearly canceled by the filling of metal−metal antibonding levels (−12 eV) (Figure 4c). If these levels were entirely of d character, the d^{10}−d^{10}

(25) Donohue, J. *The Structures of the Elements*; Wiley: New York, 1974.
(26) Pauling, L. *The Nature of the Chemical Bond*, 3rd ed.; Cornell University Press: Ithaca, NY, 1960.
(27) Lee, K.-S.; Koo, H.-J.; Dai, D.; Ren, J.; Whangbo, M.-H. *Inorg. Chem.* **1999**, *38*, 340.
(28) Koo, H.-J.; Whangbo, M.-H. *Inorg. Chem.* **1999**, *38*, 2204.
(29) Wang, M.; Mar, A. Unpublished calculations.

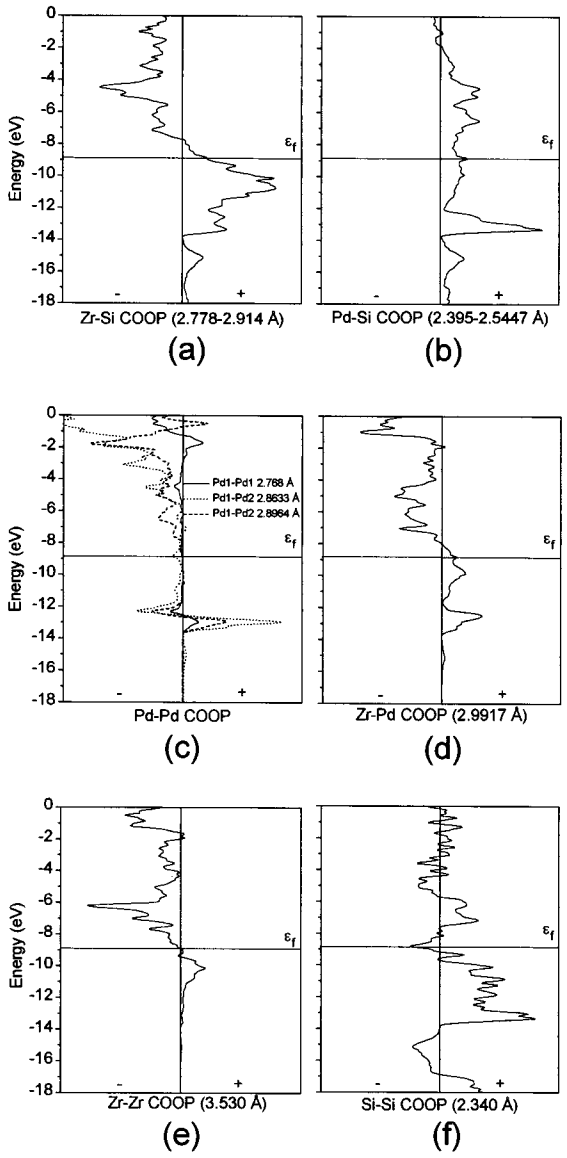

Figure 4. Crystal orbital overlap population (COOP) curves for the indicated (a) Zr−Si, (b) Pd−Si, (c) Pd−Pd, (d) Zr−Pd, (e) Zr−Zr, and (f) Si−Si contacts in $ZrPd_3Si_3$.

interaction would be repulsive. However, there is mixing of Pd 5s and 5p states which stabilizes the bonding levels sufficiently that the Pd(1)−Pd(1) interaction is net bonding (the configuration of Pd(1) determined from a Mulliken population analysis is $4d^{9.65}\ 5s^{0.36}\ 5p^{0.34}$).[30] The small but positive MOP of 0.030 for this 2.768(1) Å Pd−Pd distance is comparable to that found in elemental (fcc) Pd[25] (2.7506 Å, MOP 0.045).[29] Analysis of the other Pd−Pd contacts (∼2.9 Å) gives similar results and suggests weak metal−metal bonding. With electron-rich Pd atoms close to Zr atoms, further metal−metal bonding occurs, as shown by the filling of bonding levels in the COOP curve (Figure 4d) for the Zr−Pd(2) contact of 2.9917(8) Å, with an MOP of 0.110. The longer Zr−Pd(1) distances of 3.217(1) and 3.3149(9) Å also correspond to slightly positive MOPs of 0.047 and 0.041, respectively. Although the Zr−Zr distance of 3.530(1) Å is quite long (cf., 3.1793−3.2318 Å in elemental Zr),[25]

(30) (a) Pyykkö, P. *Chem. Rev.* **1997**, *97*, 597. (b) Dedieu, A.; Hoffmann, R. *J. Am. Chem. Soc.* **1978**, *100*, 2074. (c) Mehrotra, P. K.; Hoffmann, R. *Inorg. Chem.* **1978**, *17*, 2187.

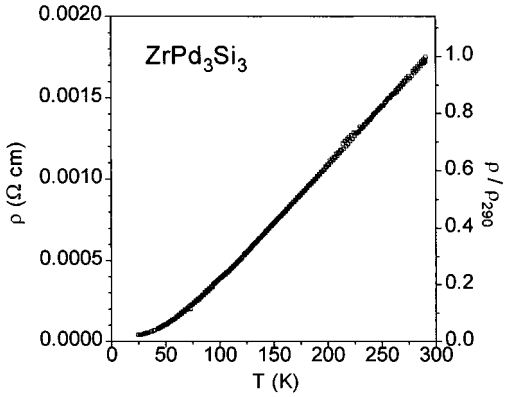

Figure 5. Resistivity vs temperature for $ZrPd_3Si_3$ ($\rho_{20} = 4.0 \times 10^{-5}$ and $\rho_{290} = 1.7 \times 10^{-3}$ Ω cm; $\rho_{20}/\rho_{290} = 0.024$).

the MOP of 0.104 and the COOP curve (Figure 4e) imply weak bonding.

The Si(1)−Si(1) pair is confirmed to be a strong homonuclear single bond resulting from overlap of mostly p and some s orbitals. Not all of the bonding levels are occupied (Figure 4f), and the MOP of 0.685 is somewhat smaller than those found in $MNiSi_3$ (M = Sm, Y) (MOP 0.827)[7a] and elemental Si (MOP 0.85),[25,29] despite similar bond lengths of ∼2.35 Å. Although Figure 2a has been drawn to emphasize the Si(1)−Si(1) pairs, there are two longer Si−Si distances that could be interrogated for bonding, given that weak bonding is implicated even at 2.8 Å in $MNiSi_3$ (M = Sm, Y). The cubic array of Si atoms is distorted so that the Si_2 pairs forming the sides are tilted. The shortest distance between these pairs is 3.055(2) Å, corresponding to an MOP of 0.186. The distance from a Si(1) atom in these pairs to an isolated Si(2) atom is 2.969(2) Å, corresponding to an MOP of 0.258. These are substantial bonds that cannot be neglected. Indeed, the 3.055(2) Å bond that straddles adjacent Si_2 pairs excludes the possibility that the apparent cavity above and below the Zr atoms could be occupied by additional atoms.

Consistent with the weakly metallic behavior observed in $ZrPd_3Si_3$ (Figure 5), the band structure shows no energy gap and only a low DOS at the Fermi level (Figure 3a). Although the resistivity measurement gives only the component along the *a* direction, $ZrPd_3Si_3$ is predicted to be a three-dimensional metal since bands are crossed in all directions in the band dispersion diagrams.

It is interesting to note that, in the Zr−Si and especially the Pd−Si COOP curves, there remain some available bonding levels above the Fermi level (Figure 4a,b). The structure may thus be amenable to accepting more electrons, at the expense of weakening the homoatomic metal−metal and nonmetal−nonmetal bonds, suggesting that compounds such as "$NbPd_3Si_3$" may be feasible targets. However, given that both metal−metal and nonmetal−nonmetal bonding provide important contributions to the stability of $ZrPd_3Si_3$, it is perhaps not surprising that even the obvious congeneric substitutions (Zr/Hf, Ni/Pd/Pt) may not be so straightforward and have thus far failed.

Acknowledgment. This work was supported by the Natural Sciences and Engineering Research Council of

Canada and the University of Alberta. We thank Mr. Michael Ferguson and Dr. Robert McDonald (Structure Determination Laboratory) for assistance in the data collection and Mr. Robert Lam and Prof. John Beamish (Department of Physics) for assistance in the resistivity measurement.

Supporting Information Available: A listing of X-ray powder diffraction data, a band dispersion diagram, and one X-ray crystallographic file, in CIF format, are available. This material is available free of charge via the Internet at http://pubs.acs.org.

CM990296B